ELSEVIER

Contents lists available at ScienceDirect

Environment International

journal homepage: www.elsevier.com/locate/envint



Full length article

A three-dimensional mouse liver organoid platform for assessing EDCs metabolites simulating liver metabolism

Ji Hyun Moon ^{a,1}, Hyun-Soo Roh ^{b,c,1}, Young Jae Park ^{a,1}, Hyun Ho Song ^a, Jieun Choi ^a, Da Woon Jung ^a, Soo Jin Park ^d, Ho Jin Park ^d, So-Hyeon Park ^e, Da-Eun Kim ^b, Gahee Kim ^{b,c}, Joong-Hyuck Auh ^e, Dong Ha Bhang ^{b,c}, Hong Jin Lee ^e, Do Yup Lee ^{a,f,g,h,*}

- ^a Department of Agricultural Biotechnology, Seoul National University, Seoul 00826, Republic of Korea
- b Department of Molecular and Cellular Biology, Sungkyunkwan University School of Medicine, Suwon, Gyeonggi 16419, Republic of Korea
- ^c Attislab Inc., Anyang, Gyeonggi-Do 14059, Republic of Korea
- d Department of Inflammation and Immunity, Lerner Research Institute, Cleveland Clinic, Cleveland, OH 44195, USA
- ^e Department of Food Science and Biotechnology, Chung-Ang University, Anseong 17546, South Korea
- f Department of Food and Animal Biotechnology, Seoul National University, Seoul 00826, Republic of Korea
- ^g Center for Food and Bioconvergence, Research Institute for Agricultural and Life Sciences, Interdisciplinary Programs in Agricultural Genomics, Seoul National University, Seoul 00826, Republic of Korea
- h Green Bio Science & Technology, Bio-Food Industrialization, Seoul National University, 1447 Pyeongchang-daero, Daehwa-myeon, Pyeongchang-gun, Gangwon-do 25354. Republic of Korea

ARTICLE INFO

Keywords: Endocrine-disrupting chemicals OECD test guideline Liver metabolism Mouse liver organoids Bioactivation

ABSTRACT

Hepatic metabolism is an important process for evaluate the potential activity and toxicity of endocrine disrupting chemicals (EDCs) metabolites. Organization for Economic Co-operation and Development (OECD) has advocated the development of *in vitro* assays that mimic *in vivo* hepatic metabolism to eventually replace classical animal tests. In response to this need, we established a 3D mouse liver organoid (mLO) platform that mimics the animal model and is distinct from existing models. We evaluated the effects the activity of EDC metabolites generated through mLOs based on human cell-based reporter gene assays in addition to existing models. This study emphasizes the importance of hepatic *ex-vivo* and suggests the need a new metabolic model through a 3D mLOs platform. These results indicate that mLOs provides a novel biological method to screen for potential endocrine-disrupting activities of EDC metabolites.

1. Introduction

Endocrine-disrupting chemicals (EDCs) are exogenous substances found in our environment, food, and various industrial products. They can interfere with the endocrine system by altering the way hormones are produced, released, transported, metabolized, or recognized by their receptors in animals, including humans (Eldridge and Laws, 2016; Heindel et al., 2017; Papalou et al., 2019; Sakkiah et al., 2018; Shanle and Xu, 2011; Tabb and Blumberg, 2006; Zoeller et al., 2012). In modern life, exposure to EDCs has increased due to industrialization, the widespread use of synthetic chemicals, and lifestyle changes, leading to a variety of health issues such as infertility and birth defects (Kahn et al., 2020; Yilmaz et al., 2020; Zlatnik, 2016). As a result, establishment of

standard methods to accurately evaluate the risk of EDCs is of great importance (Yilmaz et al., 2020).

Organization for Economic Co-operation and Development (OECD) member countries have been actively developing and establishing EDCs testing methods since 1998 (Gelbke et al., 2004; Grignard et al., 2020). Animal model has proven the practical value, including EDCs evaluation (Hass et al., 2004). Level 3 EDC testing involves *in vivo* assays to probe specific endocrine pathways and evaluate molecular mechanisms that are likely function in humans (Hass et al., 2004). However, outcomes vary according to the animal model used (e.g., mouse, rat, or rabbit), and animal testing can be a time-consuming processing (Browne et al., 2020). Furthermore, animal testing regulations are expanding globally, centered on the three Rs (Replacement, Reduction, and Refinement)

^{*} Corresponding author at: College of Agriculture and Life Sciences, Seoul National University, 1 Gwanak-ro, Gwanak-gu, Seoul 08826, Republic of Korea. E-mail address: rome73@snu.ac.kr (D.Y. Lee).

These authors contributed equally to this study.

(Maestri, 2021; Rinwa et al., 2024). The current assessment of EDCs, according to the OECD Conceptual Framework for Testing and Assessment of Endocrine Disrupting Chemicals, focuses on the impact on metabolic processes and the assessment of potential endocrinedisrupting activity by both the parent compound and its metabolites (Browne et al., 2020; Hass et al., 2004; OECD, 2012; OECD, 2018a). To this end, there is increasing demand for new ex vivo (semi in vivo) systems to evaluate the effects of potential hazardous compounds, including metabolized products (Li et al., 2014; OECD, 2018a; Ooka et al., 2020; van Vugt-Lussenburg et al., 2018). Recently, the OECD has explored the use of the S9 fraction as a potential in vitro approach to minimize the use of animals in experiments (OECD, 2018b; Reichstein et al., 2023; Zercher et al., 2024). The liver S9 fraction, which includes both microsomal and cytosolic fractions, serves as a source of drugmetabolizing enzymes, including CYP450s (J Richardson et al., 2016). Ex vivo systems have the potential to overcome the limitations of in vitro methods and also reduce animal testing based on the 3R principles.

The liver is essential for energy metabolism and xenobiotic detoxification, in addition to performing numerous endocrine functions such as direct hormone production and hormone metabolism (Rahman et al., 2022; Rhyu and Yu, 2021). Hepatic metabolism is based on Phase I (detoxification) and Phase II (conjugation) reactions; the resulting reaction products may lead to more or less active forms (Reinen and Vermeulen, 2015; Stanley, 2024; Taxak and Bharatam, 2014). Since most EDCs undergo metabolic biotransformation, their activity may vary depending on the types of metabolites produced. Therefore, it is essential to employ *ex vivo* models (e.g., animal replacement models) to assess the metabolic activity of EDCs and their metabolites (Jacobs et al., 2008; Jacobs et al., 2013).

Adult stem cell-derived 3-dimensional organoid culture systems are promising tools for disease modeling and drug development, as they have the advantages of both cell cultures and animal models. These systems have greater physiological similarity and translational potential than conventional 2D culture systems (Caipa Garcia et al., 2022; Clevers, 2016; Dutta et al., 2017; Kim et al., 2020; Skottvoll et al., 2021). Adult liver organoids possess the bi-potential to differentiate into hepatocytes and biliary epithelial cells (cholangiocytes), allowing them to recapitulate the structure and physiological functions of liver tissue (Huch et al., 2013). These systems are short-term, require a small number of animals, and can be used to evaluate the effects of chemicals as an endpoint for biologically-based assessments (Ishigamori et al., 2022). In particular, liver organoids are similar to typical livers in their differentiation and metabolic capabilities as well as mRNA expression patterns (He et al., 2020; Ramachandran et al., 2015; Vyas et al., 2018). A previous study reported that 3D-cultured hepatocytes had better liverspecific functions in terms of cytochrome P450 (CYP) activity than 2D monolayer-cultured hepatocytes (Mandon et al., 2019; Vorrink et al., 2017; Wu et al., 1999). Several studies have reported that adult liver organoid models can be applied for disease modeling and drug screening; however, their application in the assessment of EDCs has yet to be explored (Broutier et al., 2017; Elbadawy et al., 2020; Schene et al., 2020).

In the current study, we investigated mouse liver organoids (mLOs) as an evaluation system for the estrogen receptor-mediated disruption effects of EDC biotranformants. Activity assays were conducted using international standard stably transfected transactivation assay (STTA) analysis, OECD PBTG No.455, using the VM7Luc4E2 cell line (Casey et al., 2012; Chemicals, 2000; Christina, 2021). We demonstrated the potential applicability of the mLO system by comparatively analyzing the S9 fraction system, an existing metabolic model. Our findings indicate that the mLO system, in combination with metabolomics profiling and *in silico* structure prediction, can be used to assess the effects of EDCs and their metabolites. Using this model, we provide critical insights into the actual activity of EDC metabolites mediated by hepatic metabolism, and demonstrate the utility of an *ex vivo* platform and integrated evaluation pipeline as potential replacements for animal testing.

2. Materials and methods

2.1. Chemicals and standards

The following standard chemicals were selected for this study based on several OECD test guidelines; OECD TG 455 (Performance-Based Test Guideline for Stably Transfected Transactivation *In Vitro* Assays to Detect Estrogen Receptor Agonists and Antagonists) (No, 2021). The exposure range of each substance was determined according to the guidelines (Table 1). The following standard chemicals were donated by the Ministry of Food and Drug Safety (MFDS): 17beta-estradiol (E2), Diethylstilbestrol (DES), Kaempferol, Bisphenol A (BPA), Di-n-butyl phthalate (DBP), Apigenin, Butylbenzyl phthalate (BBP), p,p'-Methoxychlor, Raloxifene HCl (RAL), Tamoxifen (TAM), ICI182780, 4-hydroxy tamoxifen (4-OHT), Spironolactone (SPL), Atrazine, Corticosterone (CORT). The following chemicals were purchased from Sigma-Aldrich (USA): Estrone.

2.2. Mice

Adult liver stem/progenitor cells were isolated from 12- to 18-week-old wild-type C57BL/6 mice. Primary liver endothelial cells (LiECs) were isolated from 12- to 18-week-old GFP transgenic C57BL/6 mice (Roh et al., 2024). Control mice were fed standard pelleted food for 4 weeks. During the adaptation period, all mice were housed at 3 animals/cage with a 12-h light–dark cycle in a temperature-controlled room. Food and water were available ad libitum until the commencement of the experimental procedures.

2.3. Primary liver endothelial cell culture

LiECs were isolated from GFP transgenic mice as previously described (Roh et al., 2024). In brief, liver tissue was minced and digested in digestion solution (2.5 mg/mL collagenase type II, 100 μ g/mL DNase I) for 1 h at 37 °C. After quenching collagenase activity with an equal volume of FBS, digested cells were filtered through 100 μ m and 40 μ m strainers. To remove debris, cells were plated on a gelatin-coated cell culture dish in endothelial cell medium (ECM) and the medium was

Table 1 List of 15 EDCs.

Chemical	CAS No.	Organoid phenotype	ER STTA Conc
		Conc (M)	(M)
17ß-estradiol	50-28-2	5x10 ⁻⁶	3.67x10 ⁻⁸ -
			4.38x10 ⁻¹³
Diethylstilbestrol	56-53-1	1x10 ⁻⁶	10 ⁻⁸ -10 ⁻¹³
Kaempferol	520-18-3	1x10 ⁻⁶	3.49x10 ⁻⁵ -
			3.49x10 ⁻¹⁰
Bisphenol A	80-05-7	5x10 ⁻⁶	4.38x10 ⁻⁵ -
		6	4.38x10 ⁻¹⁰
Di-n-butyl phthalate	84-74-2	1x10 ⁻⁶	3.59x10 ⁻⁶ -
		6	3.59x10 ⁻¹¹
Apigenin	520-36-5	1x10 ⁻⁶	3.7x10 ⁻⁶ -3.7x10 ⁻
Butylbenzyl	85-68-7	1x10 ⁻⁶	3.2x10 ⁻⁵ -3.2x10 ⁻
phthalate			10
p,p'- Methoxychlor	72-43-5	4x10 ⁻⁶	2.89x10 ⁻⁵ -
		6	2.89x10 ⁻¹⁰
Raloxifene HCl	82640-04-	1x10 ⁻⁶	1.96x10 ⁻⁵ -
	8	4	1.96x10 ⁻¹⁰
Tamoxifen	10540-29-	1x10 ⁻⁶	2.69x10 ⁻⁵ -
*****	1	4.0-6	2.69x10 ⁻¹⁰
ICI182780	129453- 61-8	1x10 ⁻⁶	10 ⁻⁶ -10 ⁻¹¹
4-hydroxytamoxifen	68392-35-	1x10 ⁻⁶	10 ⁻⁶ -10 ⁻¹¹
i nydroxytamoxich	8	IAIO	10 10
Spironolactone	52-01-7	5x10 ⁻⁶	$10^{-5} - 10^{-10}$
Atrazine	1912-24-9	1x10 ⁻⁶	10 ⁻⁶ -10 ⁻¹¹
Corticosterone	50-22-6	1x10 ⁻⁶	10 ⁻⁶ -10 ⁻¹¹

replaced with fresh ECM after 4 h. Once the cells reached > 90 % confluency, the cells were processed using CD31-microbeads (Miltenyi Biotec) MACS selection according to manufacturer's protocols. LiECs were cultured and used for experiments between passages 3 and 6.

2.4. Liver organoid culture system

Adult liver stem/progenitor cells or primary liver endothelial cells (LiECs) were isolated from liver tissue of 12–18-week-old wild-type mice using a modified protocol previously described (Bhang et al., 2018). In brief, collected biliary fragments were digested in digestion solution for 30 min at 37 °C, then enzymatic activity was quenched with FBS (Gemini). The pellet was washed with basal medium (25 mM HEPES (Gibco), GlutaMAX (Gibco), MEM Non-Essential Amino Acids (Gibco), 50 U/ml penicillin, 50 μg/ml streptomycin, sodium pyruvate without phenol-red in DMEM) and 5,000 cells were mixed with 50,000 LiECs in a mixture of Matrigel (Corning). After incubation at 37 °C for 30-60 min, growth medium (basal medium supplemented with 1 % insulintransferrin-selenium (ITS, Gibco), 3 % charcoal-stripped FBS (Gemini), 5 % Knock-out serum replacement (Gibco), Endothelial Cell Growth Supplement (ECGS, 100 µg/mL, BD), heparin (50 µg/mL, Sigma), Nicotinamide (10 mM, Sigma) and Y-27632 (10 µg/mL, Tocris)) was added. Growth medium was refreshed every 3-4 days. For expansion, mouse liver organoids (mLOs) were harvested ice-cold Recovery solution (BD) and incubated at 4 °C for 30 min, then centrifuged at 400 g for 5 min. mLOs were resuspended with basal medium and mechanically disrupted, then passaged at a 1:10 ratio every 7 to 14 days.

For EDCs assessment, mechanically disrupted mLOs were incubated with TrypLE (Gibco) at 37 °C for 10 min counted with trypan blue staining. Mixture of 5,000 single cells and 50,000 LiECs in Matrigel were seeded on 24-well cell culture plate. After 4 days, 15 EDCs (Table 1) were treated for 3 days. All supernatants were harvested and analyzed for metabolic profiling and luciferase assay. DMSO (0.1 %) was used as control for EDC treated group. To assess organoid formation efficiency, the number and size of mLOs with a diameter greater than 100 μm were measured (n = 3). All bright-field images were acquired using a Thermo Evos FL Auto 2 microscope and analyzed by Celleste image analysis software.

2.5. Immunofluorescence

Whole-mount immunofluorescence staining for liver organoids was performed by previously described protocol (Roh et al., 2024). Briefly, liver organoids were harvested using Recovery solution and fixed with 10 % NBF at 4 °C for 30 min. After quenching formaldehyde with quenching solution, organoids were washed with washing solution. Organoids were permeabilized for 15 min, then blocked for 2 h at RT. After washing three times with PBST (0.1 % tween 20), organoids were incubated at 4 °C overnight with one of the following primary antibodies: rabbit anti-SOX9 (Millipore, Cat# AB5535, 1:100), rabbit anti-LGR5 (Abcam, Cat# ab75850, 1:100), rabbit anti-albumin (Abcam, Cat# ab20737, 1:100), rat anti-EpCAM (Invitrogen, Cat# 14-5791-81, 1:100), rat anti-MIC1-1C3 (Novus, Cat# NBP1-18961, 1:100), and rat anti-Ki67 (Invitrogen, Cat# 14-5698-82, 1:200). The organoids were washed three times with PBST and incubated with Alexa Flour secondary antibodies (Invitrogen) diluted in blocking buffer at room temperature for 2 h or at 4 °C overnight, then washed three times with PBST, followed by mounted with Vectashield H-1800. The immunofluorescent images were obtained using a LSM710 confocal laser scanning microscope.

2.6. Metabolites extraction for metabolic profiling

To extract metabolites, post-metabolic medium in the organoid culture (200 μ L) were added to 1 mL of extraction solvent (ACN: MeOH = 1:1, v/v). Following this, mixture was subjected to vortexing for 10 s,

sonication for 10 min, deproteinization at $-20\,^{\circ}\text{C}$ for 1 h, and centrifugation for 15 min (16,100 rcf, at 4 $^{\circ}\text{C}$). The resulting supernatant (1200 μL) was transferred and concentrated using a speed vacuum concentrator. The extracted samples were reconstituted with 50 μL of water. The procedure for treating the S9 fraction with E2 was performed following the previously referenced protocol (Jang et al., 2023; Jeon et al., 2021). In the case of mouse liver tissue, 50 mg of tissue and stainless-steel beads were placed into a 2 mL Eppendorf tube. The liver tissue was homogenized using a Mixer Mill MM400 (Retsch) at 28 Hz for 60 s. Subsequently, 1 mL of extraction solvent (ACN: MeOH = 1:1, v/v). was added, and the remaining procedures were carried out as described for the media.

2.7. Liquid chromatography-mass spectrometry (LC-MS) analysis

The reconstituted metabolites were chromatographically separated by the Ultimate-3000 ultra performance liquid chromatography (UPLC) system (Thermo Fisher Scientific, MA, USA) with a Hypersil Gold C-18 column (1.9 μm , 2.1 \times 100 mm, Thermo Fisher Scientific, MA, USA). The mobile phase of positive mode consisted of solvent A (water with 0.1% formic acid, v/v) and solvent B (ACN with 0.1% formic acid, v/v). The gradient elution was set to the following: 0-2.0 min, 10 % B; 2.0-20.0 min, 10 %-95 % B; 20.0-22.0 min, 95 % B; 22.0-22.1 min, 95 %–10 % B; 22.1–25.0 min, 10 % B. Flow rate was set to 300 μ L/min. MS analysis was performed by the Q-Exactive Plus instrument (Thermo Fisher Scientific, MA, USA) controlled by Q-Exactive Tune and Xcalibur 4.0 software. The setting parameters of heated electrospray ionization probe were as follows; S-lens radio frequency level of 50 v; HESI-II voltages of 3800 v for the positive and 3500 v for the negative; heater temperature of 300 °C; heated capillary temperature of 320 °C. The Full-MS scan were acquired over a mass range of $80-1200 \, m/z$. The Full-MS/ dd-MS2 scan was conducted using High Energy Collision Dissociation (HCD) with stepped collision energy (30, 40, and 50 eV). The maximum injection time was set 100 ms with automatic gain control (AGC) targets of 10⁶ ions.

2.8. Data processing of metabolic profiling

The raw data obtained from the LC-Orbitrap MS analysis were processed to identify the biotransformants of target compounds using Compound Discoverer (version 3.2, Thermo Fisher Scientific, San José, CA, USA) as previously described by Jeon et al. (Jeon et al., 2021). Additionally for the untargeted profiling and Global Natural Products Social Molecular Networking (GNPS) analysis, the data matrix was generated and processed using MS-DIAL (4.9.221218) software. A molecular network was constructed using the feature-based molecular network (FBMN) workflow on GNPS (Nothias et al., 2020). The precursor ion mass tolerance was adjusted to 0.01 Da, and the MS/MS fragment ion tolerance was set to 0.02 Da. In the resulting molecular network, edges were filtered to retain only those with a cosine score greater than 0.7 and more than 6 matched peaks. Missing value imputation was performed by implementing the minimum peak area value observed across the metabolite profiles.

2.9. Phase I + II biotransformation in rat liver S9 fraction

The S9 fraction mixture used for rat liver phase I + II biotransformation included 0.01 mg/ml rat liver S9 fraction, phase I cofactors (2x10 $^{\text{-}4}$ M NADPH, 3x10 $^{\text{-}3}$ M G-6-P, 5x10 $^{\text{-}3}$ M MgCl2, 0.3 units/ml G-6-PD) and phase II cofactors (2x10 $^{\text{-}3}$ M GSH, 5x10 $^{\text{-}4}$ M UDPGA, 2x10 $^{\text{-}6}$ M PAPS), co-treated with 50 μM of E2. To assess if test chemicals bound to S9 fraction proteins and induced changes in transcriptional activity, an inactive S9 fraction group containing only S9 fraction without any cofactors was employed.

2.10. RNA extraction, library preparation, and sequencing

Total RNA was extracted from liver organoid samples using the TRIzol reagent (Invitrogen, USA) according to the manufacturer's protocol. The purity and concentration of the extracted RNA were evaluated using a NanoDrop™ One/OneC spectrophotometer (Thermo Scientific, USA), with A260/A280 ratios of approximately 2.0 indicating high purity. RNA integrity was assessed using an Agilent 2100 Bioanalyzer (Agilent Technologies, USA), and only samples with an RNA Integrity Number (RIN) greater than 7 were used for further processing. RNA sequencing libraries were prepared using the TruSeq Stranded mRNA LT Sample Prep Kit (Illumina, San Diego, CA, USA), which selectively enriches polyadenylated RNA to focus on coding transcripts. Following the manufacturer's instructions, RNA was reverse-transcribed into cDNA, adapters were ligated to the cDNA fragments, and PCR amplification was performed to enrich the libraries. The quality and fragment size distribution of the amplified libraries were evaluated using the Agilent 2100 Bioanalyzer. The prepared RNA-seq libraries were sequenced at Macrogen Inc. (Seoul, Korea) using an Illumina platform. Paired-end sequencing was conducted with a read length of 101 base pairs (bp), achieving an average sequencing depth of approximately 61 million reads per sample.

2.11. RNA-seq data processing and analysis

Raw sequencing FASTQ files were assessed for quality, adapter content, and duplication rates using FastQC (v0.11.7). Adapters were removed using Trimmomatic (v0.38), and low-quality bases (Phred score < 20) along with reads shorter than 36 bp were discarded. Posttrimming quality control was performed with FastQC to ensure high data integrity before alignment. High-quality trimmed reads were aligned to the Mus musculus reference genome (GRCm38/mm10) using HISAT2 (v2.1.0) with default settings optimized for spliced read mapping. The alignment achieved an average mapping rate of 98 % across all samples. Gene expression levels were quantified using StringTie (v2.1.3b), generating read counts, fragments per kilobase of transcript per million mapped reads (FPKM), and transcripts per kilobase million (TPM) for each gene. Raw read counts were normalized using the Trimmed Mean of M-values (TMM) method to adjust for differences in library size across samples. Differential expression analysis was conducted using the edgeR package, with genes exhibiting an absolute log2 fold change > 2 and a raw p-value < 0.05 considered significantly differentially expressed. Functional enrichment analysis was performed using g, focusing on Gene Ontology (GO) terms to identify biological processes, molecular functions, and cellular components significantly associated with the differentially expressed genes (DEGs).

2.12. Cell lines and stably transfected transactivation assay

VM7Luc4E2 cells were obtained from MFDS. The maintenance of VM7Luc4E2 cells was carried out according to the relevant OECD test guidelines (No, 2021). The VM7Luc4E2 cell line was maintained in Roswell Park Memorial Institute 1640 (RPMI 1640) supplemented with 8 % FBS and 1 % P/S. For the stably transfected Transactivation assay, VM7Luc4E2 cells were conditioned in phenol red free DMEM supplemented with 4.5 % charcoal-stripped FBS, 1.9 % L-glutamine and 1 % P/S for 24 hr. Conditioned cells were seeded in 96-well plate (40,000 cells/well), treated with test substances for 24 hr, and luciferase activity was measured using Steady-Glo ® luciferase assay reagent (Promega).

2.13. Data analysis of luciferase assay

In the ER transcriptional activity agonist test, substances that induce an effect equivalent to more than 20 % of the effect of the positive control group (1.84×10^{-10} M E2) according to PBTG 455 were classified as ER agonist positive. All groups shared PC ago control for statistical

processing. Additionally, logPC50 concentrations are provided to help determine the strength and relative efficacy of the test chemical. The logPCx value can be calculated by interpolating between 2 points on the X-Y coordinate, one immediately above and one immediately below a logPCx value. Where the data points lying immediately above and below the logPCx value have the coordinates (c, d) and (a, b) respectively, then the logPCx value may be calculated using the following equation: log [PCx] = log [c] + (x-d)/(d-b). All data were analyzed after excluding toxic concentrations affecting cell viability or morphology through visual inspection. All data represent the mean values from three independent experiments conducted on different days, with each experiment performed in triplicate wells.

2.14. Statistical analysis

Statistical significance levels between groups across all tests were calculated using the LMSstat package (github.com/daehwankim1 2/LMSstat) in R (version 4.4.1). Student's t-test was employed for comparisons between two groups, while Analysis of Variance (ANOVA) was utilized for comparisons involving three or more groups. The adjusted p-value was calculated using the Benjamini-Hochberg approach. The normality and homogeneity of variance for each feature used in comparisons were verified using the Shapiro-Wilk test (shapiro.test) and variance test (var.test), respectively. Principal Component Analysis (PCA) visualization was implemented using the ggbiplot library, with additional ellipse representations generated through the ggforce library. For Principal Coordinates Analysis (PCoA), distances were calculated using the vegdist function from the vegan package (version 2.6-6.1), applying the Manhattan distance method. Subsequently, between-group distances of centroids were computed using the betadisper function. The circular heatmaps were generated using the circos.heatmap function from the ComplexHeatmap package (version 2.20). volcano plots were created using the Volcano function from the LMSstat package.

3. Results

3.1. Development of mouse liver organoid culture

We first established mLOs using a protocol with minimal modification from a previous study to assess the effects of EDCs. This protocol includes the use of DMEM without phenol red, which interferes with luminescence signals (Roh et al., 2024). mLOs were successfully cultured in modified culture medium, with an organoid formation efficiency of approximately 3 % (Fig. 1A, B). Consistent with our previous study, we consistently observed stable organoid formation and expansion during serial passaging of mLOs, with no significant changes in morphology or growth characteristics throughout long-term culture (12 passages in 90 days, Fig. 1C). Throughout the 12 passage, the mLOs exhibited no significant changes in structure, maintaining stable expansion and morphology. Furthermore, the expression of Lgr5 and Sox9 (stem/progenitor cell markers), EpCAM and MIC1-1C3 (biliary epithelial cell markers), and Ki67 (a proliferation marker) remained stable, with only a small subset of mLOs expressing albumin (a hepatocyte marker) (Fig. 1D). We determined the proper concentration of EDCs, considering the criteria as follows: positive control for ER agonistic STTA assay, limit of detection (LOD) of parent compounds, detectability of metabolized compounds, and cellular toxicity. We first optimized the biotransformation time with 184 pM of E2, the positive control concentration in the PBTG455. Estrogenic activity did not change until 24 and 48 h; however, estrogenic activity showed a significant decrease after 72 h of biotransformation (Fig. 1E). Seventy-twohour treatment with E2 at various concentrations did not affect organoid morphology or growth (Fig. 1F).

Subsequently, we conducted RNA sequencing to evaluate the liver metabolism-related gene expression profile of mLOs and E2 (184 pM)-

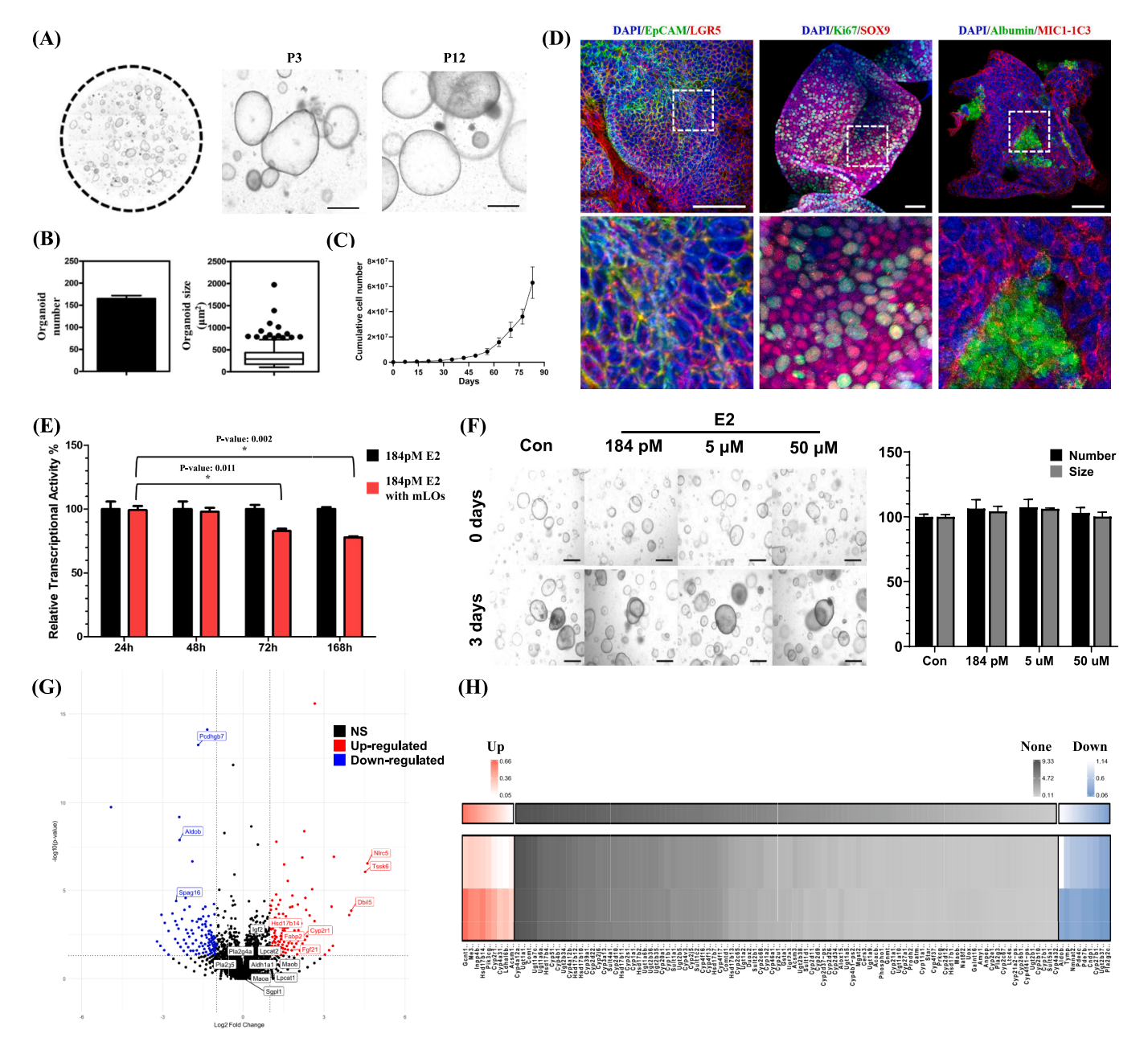


Fig. 1. Optimization and development of mouse liver organoid 3D culture system. (A) Representative stitched (left) and 4X (right) images of liver organoids at passages 3 and 12. Scale bar, μm (right). (B) Quantification of organoid-forming number and average organoid size (diameter > 100 μm). Data are means \pm standard error of the mean (SEM). Data were presented as box plot of the median and rang of organoid size. The top and bottom of the box 25th percentile and 75th percentile. The whiskers indicate minimum and maximum excluding outliers, and outliers present as circles. (C) Cumulative cell number of mLOs from P0 to P12. Data are means \pm SEM. Scale bar, 500 μm (n = 3). (D) Immunofluorescent staining for LGR5, EpCAM, SOX9, Albumin, MIC1-1C3, and Ki67. Scale bar, 50 μm. (E) The effect of E2 metabolites in VM7Luc4E2 cell lines with different treatment time using mouse liver organoids. The 184 pM E2 was treated at different time point of 24, 48, 72, and 168 hr utilizing mouse liver organoids. Data is presented by means \pm SEM (*: p-value < 0.05, one-way ANOVA with scheffe multiple comparison test) (n = 3). (F) Representative bright field images and average fold change in number and size of mLOs before and after 3 days of E2 treatment. Scale bar, 500 μm (n = 3). (G) The differential gene expression in mLOs + E2 (50 μM) group compared to mLOs group using volcano plot. The significantly different data points (p-value < 0.05, fold change > 2) are marked in red (up-regulated in mLOs + E2 group) and blue (down-regulated in mLOs + E2 group) and the others are marked in black (p-value > 0.05, fold change < 2) (n = 3). (H) The list of genes associated with E2 metabolism was analyzed by comparing the mLOs group to the mLOs group treated 184 pM E2. Gene expression levels were quantified using Transcripts Per Million (TPM), and the log2 (fold-change) values were calculated. These changes were visualized through a gradient color scheme. Genes significantly upregulated in the mLOs are shown in red, while those downreg

treated mLOs. A total of 17,952 genes were selected, of which 888 differentially expressed genes (DEGs) were detected (p value < 0.05); 180 of these were up-regulated while 162 were down-regulated based on a fold-change of more than two (Fig. 1G). Among the DEGs, *Nlrc5*, *Tssk6*, and *Dbil5* were the most significantly up-regulated genes, while

Aldob, Spag16, and Pcdhgb7 exhibited the greatest down-regulation following E2 treatment. Notably, genes related to lipid and amino acid metabolism were identified, including fatty acid-binding protein 2 (Fabp2) and fibroblast growth factor 21 (FGF21). FGF21, primarily expressed in the liver and adipose tissue, exerts its effects through FGFR receptors,

influencing the enterohepatic circulation of bile and regulating glucose and lipid metabolism (Dolegowska et al., 2019; Falamarzi et al., 2022). Although no significant differences were observed between E2stimulated and unstimulated mLOs, the presence of key metabolic enzymes such as FASN and LpCat was confirmed, further demonstrating the functional capability of mLOs to recapitulate essential liver metabolism pathways. Additionally, mLOs expressed insulin-like growth factor II (IGF-II). This gene is predominantly produced in the liver and plays a critical role in mammalian growth, metabolism, and tissue maintenance, underscoring the physiological relevance of mLOs in modeling liverspecific metabolic processes (Livingstone and Borai, 2014; O'Dell and Day, 1998). The expression of key metabolic enzymes involved in E2 biotransformation was confirmed, including CYP450, 17β-hydroxysteroid dehydrogenase (HSD17B), and sulfotransferases (SULTs). Notably, CYP2r1 and HSD17b14 were significantly upregulated by 3.92-fold and 2.56-fold, respectively, following E2 treatment of mLOs.

Expression of several other enzymes involved in phase II metabolism, such as uridine 5'-diphospho-glucuronosyltransferases (UGTs) and glutathione-S-transferase alpha 1 (GSTA1), was also detected in both E2-treated and untreated mLOs (Fig. 1H, Table S1). These genes play a significant role in detoxification, hormone metabolism, processing of endogenous and exogenous metabolites, despite of lack of differential expression following E2 treatment. Expression of metabolic-related genes in mLOs suggests that they can effectively mimic hepatic metabolism, making them a valuable model for further metabolic profiling studies (Almazroo et al., 2017).

3.2. Evaluation of the metabolic potential of mouse liver organoids based on comprehensive metabolomics

To assess the extent to which organoids mimic in vivo metabolism, we compared the metabolic capacity of rat liver tissue, mLOs, and the S9 fraction. Using principal coordinate analysis (PCoA) based on the Manhattan distance, we visualized the relationships between the metabolic profiles of the three groups (Fig. 2A, Fig. S1). A total of 113, 109, and 49 metabolites were identified in liver tissue, mLOs, and S9 fraction, respectively. When analyzing detected metabolites across liver tissue and the two metabolic models, no significant difference was observed between liver tissue and mLOs (Fig. 2A). In contrast, the S9 fraction exhibited significant differences not only compared to liver tissue but also to mLOs. When performing distance analysis using all $201\,$ metabolites identified across all groups, significant difference was observed between liver tissue and mLOs (Fig. S1). However, consistent with the earlier results, mLOs demonstrated a metabolic profile more similar to liver tissue than the S9 fraction, indicating that mLOs more closely mimic in vivo hepatic metabolic capacity than the S9 fraction.

Metabolites associated with amino acid and lipid metabolism were identified, with a total of 44 metabolites found in liver tissue, the highest number found among the groups. mLOs and the S9 fraction contained 38 and 13 metabolites, respectively. Choline exhibited the highest intensity in liver tissue, followed by mLOs and the S9 fraction (Fig. S2). Most metabolites associated with amino acid metabolism demonstrated comparable intensity levels between liver tissue and mLOs; however, they were not detected in the S9 fraction.

We evaluated the metabolic potential of mLOs in comparison to the well-established *in vitro* metabolic model, the rat liver S9 fraction. S9 fraction, consisting of liver enzymes and cofactors, offers the advantage of separately assessing phase I and phase II metabolism (J Richardson et al., 2016; Registre and Proudlock, 2016). For comparative analysis, we conducted biotransformation, including phase I + II reactions. The metabolic rate was calculated based on the intensity of unmetabolized E2. Metabolic rate of mLOs was significantly higher (37.85 %) than that of the S9 fraction (8.63 %) (Fig. 2B, Fig. S3).

Untargeted metabolomics identified a total of 118 metabolites in the without mLOs (parent) treated with 50 μM E2 and mLOs treated with 50 μM E2. In contrast, the S9 without cofactors (S9 inactive) with 50 μM E2

and the S9 Phase I + II with 50 μ M E2 resulted in the identification of 54 metabolites. PCA plot demonstrated a clear separation based on E2 biotransformation potential, distinguishing metabolites derived from mLOs and s9 fraction (Fig. 2C). PCA results indicates that the mLOs and S9 fraction metabolized E2, forming distinct biotransformation products not present in the control samples (R2X = 0.786 for mLOs, R2X = 0.780 for S9 fraction).

In mLOs treated with 50 μM E2, 20 metabolites were significantly upregulated, while four metabolites were downregulated compared to the parent treated with 50 μM E2 (Fig. 2D). In the S9 Phase I + II with 50 μM E2 compared to the S9 inactive with 50 μM E2, eight metabolites were significantly upregulated, while no metabolites were downregulated. E2 was significantly reduced exclusively in mLOs, reflecting a higher metabolic rate for E2 in mLOs than the S9 fraction. Notably, E2-related metabolites such as estrone, estriol, ethynylestradiol, and 2-methoxyestradiol were only detected and significantly increased in mLOs (Fig. S4). Among the metabolites identified only in the S9 fraction, several phase I and II cofactors necessary for S9 fraction activation, were detected.

Potential biotransformants were determined using untargeted metabolic profiling coupled to an in silico prediction algorithm. For prediction, we employed the 'Generate Expected Compounds' tool in Compound Discoverer. A total of 45 biotransformants were identified in mLOs (Table S2), among which 12 biotransformants were commonly found in the S9 Phase I + II (Fig. S5). Biotransformants increased significantly with desaturation in both mLOs and S9 Phase I + II compared to their respective controls, while dehydration transformants decreased significantly in mLOs only. Acetylation and reduction-acetylation biotransformants were increased in mLOs but decreased in S9 Phase I + II. Conversely, biotransformants with reduction-glycine conjugation, hydration, and oxidation-GSH conjugation were decreased in mLOs but increased in the S9 Phase I + II. Both metabolic models demonstrate basic metabolic capabilities through common biotransformants. However, mLOs exhibited a broader and more diverse range of biotransformants than the S9 fraction (Fig. 2E). Notably, mLOs exclusively produced biotransformants involved in key phase II detoxification pathways commonly observed in vivo, including glucuronide conjugation, cysteine conjugation, and sulfation. By contrast, more restricted metabolic pathways were observed in the S9 fraction, with GSH conjugation, driven by the phase II cofactor GSHreduced, particularly prominent.

In addition, we used Global Natural Products Social Molecular Networking (GNPS) to map metabolic features with structural similarity inferred from tandem mass spectrometry (ms/ms) (Fig. 2F, Table S3) (Gicquel et al., 2024; Nothias et al., 2020). Each node represents a metabolic feature and each edge connects to features when spectral similarity is higher than 70 %. Pie charts within each node indicate the relative abundance of the metabolic feature in different systems: parent (black), mLOs (red), S9 inactive (grey), and S9 Phase I + II (yellow). Additionally, we performed database-based structure prediction using SIRIUS's CSI:FingerID to validate features connected in the network. Most biotransformants were detected at significantly higher levels in mLOs than the S9 Phase I + II. In contrast, nodes M6 and M7 exhibited similar levels in both mLOs and S9 Phase I + II. M9 and M18 were detected at higher levels in S9 Phase I + II than in mLOs. A broader range of biotransformants were identified in mLOs than S9 Phase I + II. Notably, oxidation-related biotransformants, which are metabolized by phase I CYP1A2 enzymes, were identified only in mLOs (Table S2, Table S3) (Yamazaki et al., 1998). Glucuronidation conjugations, which are metabolized by the phase II enzyme UGT1A10, were detected only in the mLOs (Itäaho et al., 2008). The mRNA expression of CYP1A2 and UGT1A10 was detected in mLOs, and the resulting biotransformants were also identified (Table S1, Table S2). These results suggest that mLOs retain liver metabolic activity, including phase I and II activity, and possess a metabolic capability that is more similar to the in vivo system than the S9 fraction.

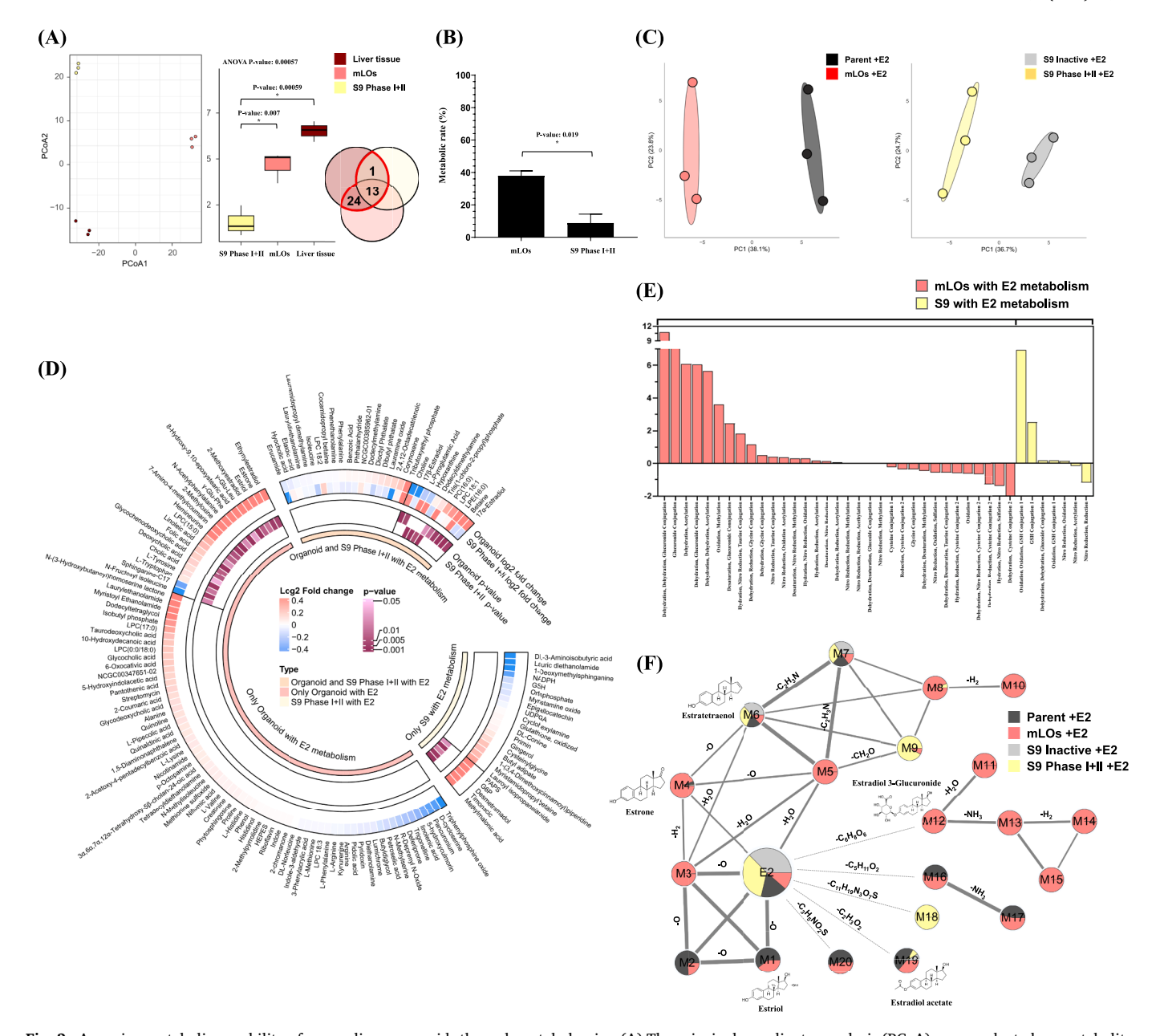


Fig. 2. Assessing metabolic capability of mouse liver organoids through metabolomics. (A) The principal coordinates analysis (PCoA) was conducted on metabolites using the Manhattan distance method and spatial median for distance to centroid across three groups: Liver tissue, mLOs, and S9 Phase I + II. Each color in the figure represents three groups. The Venn diagram depicts the number of metabolites used to calculate the groups' distances (one-way ANOVA with scheffe multiple comparison test) (n = 3). (B) Comparative metabolic rates between mLOs and S9 Phase I + II groups with treated 50 µM of E2. Data is presented by means ± SEM (*: p-value < 0.05, student t-test) (n = 3). (C) Principal component analysis (PCA) score plots comparing metabolic profiles of mLOs (left) and S9 fractions (right) treated with 50 µM E2. The left plot shows the PCA scores for the mLO group, with ellipses representing the parent (50 µM E2 without mLOs, black) and mLOs + E2 (50 µM, red) (R2X = 0.786). The right plot shows the PCA scores for the S9 fraction group, with ellipses representing the S9 inactive (S9 fraction without cofactors treated 50 μ M E2, gray) and S9 Phase I + II + E2 (50 μ M E2 with phase I + II cofactors, red) (R2X = 0.780) (n = 3). (D) The circos heatmap illustrated the changes in key metabolites in both Organoid and S9 Phase I + II models, with and without 50 µM E2 treatment. The metabolites were categorized based on their presence in either model or shared between both: those common to both Organoid and S9 Phase I + II with E2 metabolism, those specific to Organoid with E2 metabolism, and those specific to S9 Phase I + II with E2 metabolism. The log2 fold change values are depicted using a color gradient that transitions from blue to red as the values increase. The statistical significance of differences is depicted by purple color intensity gradients, displayed only for p-values less than or equal to 0.05. Metabolites exhibiting statistically significant differences were segregated and clustered unidirectionally (p-value < 0.05, student t-test) (n = 3). (E) The biotransformants identified specifically in mLOs with E2 metabolism (red) and S9 with E2 metabolism (yellow) were illustrated using stacked bar plot. The y-axis represents the log2(fold change) in the relative abundance of each biotransformant. (F) FBMN based on mLOs and S9 fraction platform for E2. Nodes represent metabolic features, and edges connect nodes with a cosine similarity of 70 % or higher. Edge thickness represents the cosine similarity between nodes, with thicker edges indicating higher similarity values. The molecular formulas annotated on the edges represent the compounds that differentiate between the connected nodes. The pie charts in each node indicate the relative abundance of the respective feature. Nodes not connected to E2 (dotted line) have lower similarity to E2 but are included as potential biotransformant candidates identified through the compound discoverer tool. The structures were predicted using CSI:FingerID. (For interpretation of the references to color in this figure legend, the reader is referred to the web version of this article.)

3.3. Proficiency test for the STTA assay using VM7Luc4E2 cell line

Proficiency tests were conducted in triplicate using reference chemicals according to OECD test guidelines (Table 2). For the agonist assay, the proficiency test met the acceptable criteria with fold-induction values of 24.0, 20.3, and 25.5 at 184 pM E2. Additionally, the proficiency test was conducted on positive reference chemicals (BPA and BBP) and a negative reference chemical (SPL). PC20 and PC50 values for the reference chemicals were consistent with the responses expected according to OECD test guidelines.

3.4. Effect of EDCs on the morphology of mouse liver organoid

Seven ER agonists-positive (DES, Kaempferol, BPA, DBP, Apigenin, BBP and p,p'-Methoxychlor) and the other seven EDCs classified as ER agonist negative, selective estrogen receptor modulator (SERM), and others (RAL, TAM, ICI 182780, 4-OHT, SPL, Atrazine and CORT) were selected from those listed in the OECD test guidelines. mLOs were treated with these EDCs for 72 h to examine if morphological changes occurred (Fig. 3). Exposure to all EDCs did not result in significant changes in the size and number of mLOs, as determined by ANOVA with a post-hoc test.

3.5. Estrogenic agonistic effects of EDCs due to mouse liver metabolism as evaluated by STTA assay using the VM7luc4E2 cell line

Estrogen-disruption activity of 15 EDCs was evaluated by ER agonistic STTA assay using the VM7Luc4E2 cell line. Visual scoring at all concentrations showed no toxicity for all EDCs tested. Concentration-response curves from the ER agonistic STTA assay quantifying estrogenic activity of EDCs and their metabolites are given in Fig. 4. PC20 and if possible, PC50 were determined through the concentration-response curves.

Out of the 15 chemicals evaluated, eight (E2, DES, kaempferol, BPA, DBP, apigenin, BBP, p,p'-methoxychlor) were determined to be agonist-positive after mLO metabolism based on pC20 values (Fig. 4, Table 3). Among them, kaempferol and BBP showed a significant reduction in estrogen-disruption activity, to the extent that PC50 values could not be determined. Estrogenic activity of five EDCs (E2, kaempferol, BPA, DBP, BBP) decreased with mLO biotransformation, while the activity of DES

Table 2Proficiency test for VM7Luc4E2 STTA assay.

Agonist test	log [PC20 ^a]		log [PC50 ^b]		
	Acceptable criteria	Results	Acceptable criteria	Results	
Bisphenol A	Positive	-7.02	Positive	-6.47	
		-7.01		-6.42	
		-7.03		-6.45	
Butylbenzyl phthalate	Positive	-5.57	Positive	-5.05	
		-6.05		-5.40	
		-6.02		-5.34	
Spironolactone	Negative	_c	_	_	
		_	_	_	
		_	_	_	
Fold induction of E2	Acceptable criteria		Results		
	>4		24.0		
			20.3		
			25.5		

 $^{^{\}rm a}$ Concentration of a test chemical at which the measured activity is 20 % of maximum activity induced by the 184 pM E2.

increased. For S9 biotransformation, two EDCs (BPA, DBP) showed increased estrogenic activity, while p,p'-methoxychlor showed decreased estrogenic activity. Agonistic negative EDCs showed no activity after biotransformation in either biotransformation model.

4. Discussion

Our current study developed an EDC evaluation system based on liver organoid culture and advanced mass spectrometric analysis, which may allow for a more precise evaluation of EDC activity with highthroughput analysis. We introduce an approach using the mLO platform, which was designed to address the limitations of in vitro metabolism applications and to more accurately mimic in vivo metabolism. The mLO platform can be used to gain insights into the molecular mechanisms of liver metabolism, potentially advancing endocrine disruption research. Our study provided insights into the biotransformation of EDCs by mLOs and their consequent estrogenic activity using a human cell-based reporter gene assay. The mLO platform, compared to traditional in vivo methods, has several distinct advantages: 1) it significantly reduces the number of animals needed for experiments in accordance with the 3R principles, 2) it enables rapid large-scale drug screening, and 3) it provides bioinactivation insights not easily obtained in vivo by directly comparing non-metabolized parent compounds with their metabolites (Ogoke et al., 2021; Park et al., 1994; Uetrecht, 2003; Yang et al., 2023). We confirmed the potential of our new ex vivo model through comparison with existing metabolic models. However, the scope of our evaluation focused on the applicability of the new ex-vivo model, and we recognized the need for future research for antagonist

Liver is a key organ responsible for various metabolic processes, including the metabolism of carbohydrates, lipids, amino acids, hormones, and biotransformation of xenobiotics (Blanco and Blanco, 2017). To mimic these diverse hepatic functions, we utilized hepatobiliary organoids co-cultured with hepatobiliary duct cells and primary murine liver endothelial cells. Metabolic capability of the mLOs was demonstrated based on the expression of key genes and the production of relevant metabolites. Expression of genes encoding enzymes involved in phase I and II metabolism, such as CYPs and UGTs, coupled with the identification of various biotransformants, suggests that MLOs closely mimic liver-specific metabolic processes. Moreover, mLOs also presented the potential to replicate a wide range of liver functions. Detection of the expression of genes such as MaoA, MaoB, and Aldh1a1 suggests that mLOs are capable of amino acid metabolism. Beyond mere gene expression, the functional implication as enzymatic activity was suggested by the metabolite profile. While direct measurements of enzymatic activity were not conducted, the detection of key metabolites—such as L-tryptophan, L-tyrosine, proline, and L-methionine—demonstrated that the gene products were correctly translated and functioned as active enzymes within the mLO environment (Denk et al., 2019; Pearl, 2013; Yang et al., 2022). Also, genes linked to lipid metabolism (e.g., FGF21, LPCATs, Pla2g4a, Pla2g5, and Sgpl1) were expressed and essential lipid metabolites (e.g., choline, LPE, and sphingolipids) (Dolegowska et al., 2019; Falamarzi et al., 2022; Wang and Tontonoz, 2019). These findings highlight that mLOs not only express key metabolic genes but also produce relevant metabolites.

In contrast, the S9 fraction did not produce these hepatic metabolites. Liver S9 fraction effectively represents phase I and II metabolism, but requires additional cofactors for functional completeness (J Richardson et al., 2016; Jia and Liu, 2007; Registre and Proudlock, 2016). Cofactors remain present after metabolism and experimental applications, which may introduce potential errors in the interpretation of results. In particular, the cofactors NADPH, G6P, UDPGA, GSH, and PAPS remain present after metabolism and experimental application. In our analysis, γ -glutamyl amino acids, such as γ -glutamylleucine (γ -Glu-Leu) and γ -glutamylphenylalanine (γ -Glu-Phe), were detected in both liver tissue and mLOs, but not in the S9 fraction. These metabolites,

^b Concentration of a test chemical at which the measured activity is 50 % of maximum activity induced by the 184 pM E2.

^c Negative activity. No activity exceeding 20 % of the 184 pM E2 value was observed up to the highest tested concentration of the test substance.

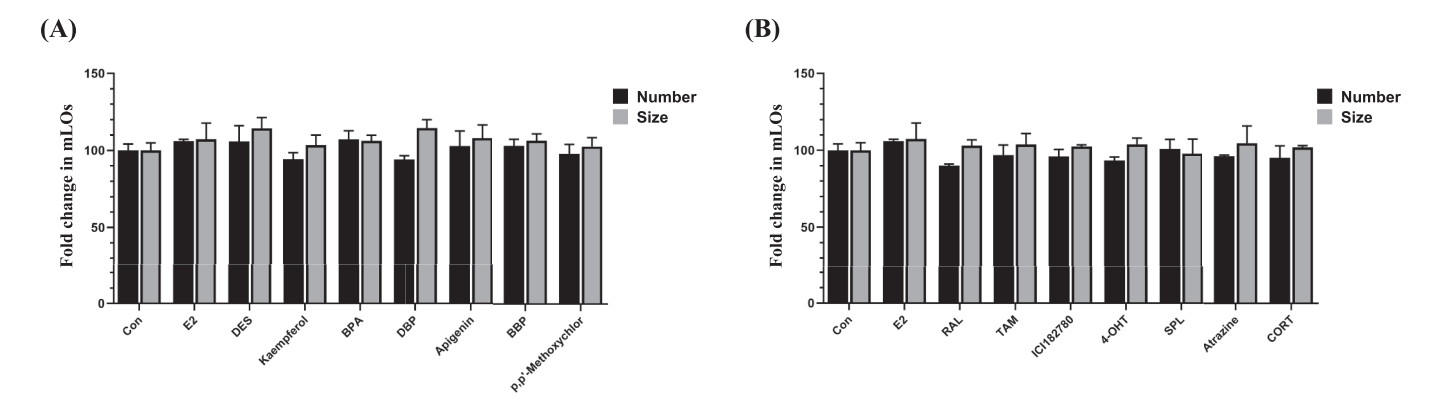


Fig. 3. Effects of EDCs treatment on mLOs number and size. Fold change values for number and size of EDC treatment compared to control over 72 h. ER agonist positive EDCs: DES, Kaempferol, BPA, DBP, Apigenin, BBP and p,p'-Methoxychlor. ER agonist negative EDCs: RAL, TAM, ICI 182780, 4-OHT, SPL, Atrazine and CORT. (A) Organoid number and size after treatment with ER agonist positive EDCs, (B) Organoid number and size after treatment with ER agonist negative EDCs. The bar plots indicate means \pm SEM (*: p-value < 0.05, one-way ANOVA with scheffe multiple comparison test) (n = 3).

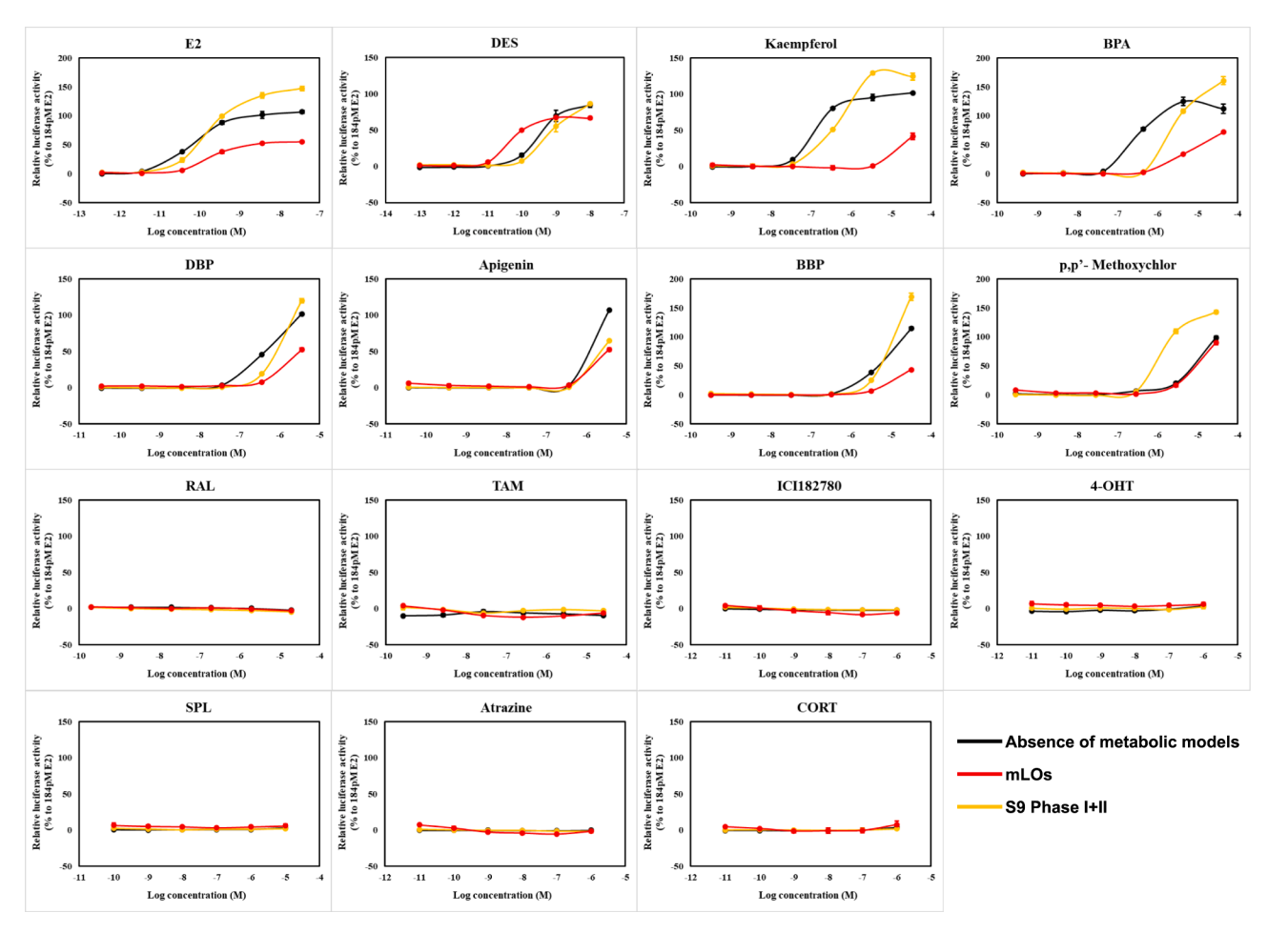


Fig. 4. ER agonist activity of EDCs metabolites in VM7luc4E2 cells using mLOs and S9 Phase I + II metabolic models. The ER transcriptional activity of each EDCs was expressed as luciferase activity relative to positive control (184 pM E2). The black line represents the activity of the EDCs in the absence of metabolic models, the red line shows the activity of EDCs metabolized by mLOs, and the yellow line represents EDCs metabolized by the rat liver S9 fraction. Data are expressed as the mean \pm SEM (n = 3). (For interpretation of the references to color in this figure legend, the reader is referred to the web version of this article.)

which are naturally present in the liver, require the activity of $\gamma\text{-glutamyltransferase}$ (GGT) enzymes. GGT enzymes are membrane-bound, located on the external surface of hepatocyte membranes, and play a crucial role in the gamma-glutamyl cycle, which is involved in amino acid transport and glutathione metabolism (Orlowski and WILK, 1975; Rahimi-Pour et al., 1986). Since the S9 fraction lacks intact cell

membranes and membrane-bound enzymes, it was unable to produce γ -glutamyl amino acids. This limitation of the S9 fraction underscores its constraints in modeling liver metabolism, highlighting the advantages of organoids as a more comprehensive metabolic model.

mLOs metabolized E2 more efficiently than the S9 fraction, and generated a more diverse range of biotransformants than the S9 fraction.

Table 3PC20 or PC50 values in VM7Luc4E2 STTA assay for EDCs in the absence and presence of metabolic models.

EDCs	Absence of metabolic models		mLOs				S9 Phase I + II			
	PC20	PC50	PC20		PC50		PC20		PC50	
	log (M)	log (M)	log (M)	FCa	log (M)	FC	log (M)	FC	log (M)	FC
E2	-10.97	-10.20	-9.99	9.55	-8.61	38.90	-10.63	2.19	-10.09	1.29
DES	-9.92	-9.36	-10.69	0.17	-9.95	0.26	-9.74	1.51	-9.11	1.78
Kaempferol	-7.31	-6.89	-4.99	208.93	_b	_	-7.11	1.58	-6.49	2.51
BPA	-7.14	-6.73	-5.80	21.88	-4.94	61.66	-6.20	8.71	-5.91	6.61
DBP	-7.06	-6.37	-6.17	7.76	-5.60	5.89	-6.44	4.17	-6.14	1.70
Apigenin	-6.27	-5.98	-6.17	1.26	-5.76	1.66	-6.13	1.38	-5.66	2.09
BBP	-6.01	-5.35	-5.14	7.41	_	_	-5.72	1.95	-5.32	1.07
p,p'- Methoxychlor	-5.75	-5.15	-5.60	0.48	-5.06	1.23	-6.40	0.08	-6.11	0.11
RAL	_	_	_	_	_	_	_	_	_	_
TAM	_	_	_	_	_	_	_	_	_	_
ICI182780	_	_	_	_	_	_	_	_	_	_
4-OHT	_	_	_	_	_	_	_	_	_	_
APL	_	_	_	_	_	_	_	_	_	_
Atrazine	_	_	_	_	_	_	_	_	_	_
CORT	_	_	_	_	_	_	_	_	_	_

^a FC: Fold change compared with absence of metabolic models.

The significant increase in estriol in mLOs is an important indicator that mLOs successfully performed phase I metabolism. mLOs exhibited no significant changes in the expression levels of CYP such as *Cyp3a13*, *Cyp1a1*, and *Cyp1b1*; however, they successfully generated the significant amounts of estriol, the product of E2, through effective Phase I oxidative metabolism (Lazier, 1963). Furthermore, the expression of various enzyme families, including UGTs and SULTs, indicates that mLOs are capable of conducting multiple conjugation reactions (Longcope et al., 1985). Identification of estradiol 3-glucuronide through GNPS analysis supports the active involvement of mLOs in phase II metabolism. Additionally, the expression of *catechol-O-methyl-transferase* (*Comt*) involved in the methylation pathway, along with the identification of methoxyestradiol, suggests that mLOs can effectively mimic Phase II metabolism (Parada-Bustamante et al., 2015).

mLOs act as a platform for hepatic metabolism, and any damage or growth impairment of mLOs during EDC treatment may lead to distorted or inaccurate interpretation of metabolic capability. To address this, we examined if there were morphological changes in mLOs after EDC exposure; we observed no significant differences across treatments. Absence of morphological alterations indicates that mLOs maintain their structural integrity when exposed to EDCs, allowing them to sustain metabolic activity without cellular damage, toxicity, or disruption.

STTA assay uses the VM7Luc4E2 cell line, which was derived from the MCF7 human breast cancer cell line that endogenously express both human ER forms, ERα and Erβ (Casey et al., 2012). PC20 and PC50 values of E2 activity were increased by mLO biotransformation (9.55fold and 38.9-fold, respectively), in contrast to no significant changes in these values after phase I + II metabolism in the S9 fraction. Approximately 37.85 % of E2 was metabolized by mLO biotransformation, whereas about 8.63 % was metabolized by the S9 Phase I + II. These results indicate that the differential estrogenic activity of mLOs and S9 Phase I + II was due to different levels of remaining E2 between the two biotransformation approaches. Estrogenic activity of E2 was significantly lower in mLOs, corresponding to their larger metabolic rate, than the S9 fraction. Also, estrone level was much higher after mLO biotransformation than the S9 Phase I + II (Fig. S6). Estrone, reported as a major compound metabolized from E2, has a lower ER binding capacity, compared to E2 (Adamski et al., 1995; Hilborn et al., 2017; Kuhl, 2005; Labhart, 2012; Nokelainen et al., 1998; Van den Belt et al., 2004). Estrone generated from mLO biotransformation contributes to estrogenic activity. Additionally, HSD17B was reported to metabolize E2 into estrone (Adamski et al., 1995; Hilborn et al., 2017; Nokelainen et al., 1998). E2 treatment in mLOs resulted in approximately 2.56-fold upregulation of HSD17B14 gene expression level. The estrogenic

activity reveals complex interactions among the metabolic rates, metabolites, and biotransformation by mLOs.

The generation of metabolites through hepatic biotransformation has a critical influence on the activity changes of EDCs. BPA had lower estrogenic activity in both mLOs and S9 Phase I + II after biotransformation than the parent compound. BPA has been reported to undergo substantial biotransformation (e.g., glucuronide conjugation and sulfation) in rat hepatic microsomes and hepatocytes (Elsby et al., 2001; Ho et al., 2017; Inoue et al., 2016). Previous studies showed that the estrogenic activity of BPA metabolites was significantly lower than that of BPA, consistent with our experimental findings. Interestingly, BPA metabolites of mLOs had lower activity than S9 Phase I + II BPA metabolites. Both metabolic models displayed the biotransformation activities of glucuronide conjugation and sulfation; however, more diverse types of biotransformation were present in mLOs than in S9 Phase I + II (Table S4). Through a comprehensive analysis of the results, differential estrogenic activity may be explained by the different levels of biotransformants produced in mLOs.

In summary, our current result proposed a promising strategy for 1) high-throughput screening of compounds with ER agonistic activity, allowing closer proximity to *in vivo* event by 3D organoid and 2) systematic identification of key metabolic features, which may lead to a comprehensive understanding of the mode of action.

5. Data statement

Raw data is available at the Korea BioData Station (K-BDS, https://kbds.re.kr/) under the accession ID KAP240925.

CRediT authorship contribution statement

Ji Hyun Moon: Writing – original draft, Validation, Investigation, Conceptualization. Hyun-Soo Roh: Validation, Methodology, Investigation. Young Jae Park: Writing – original draft, Visualization, Formal analysis, Data curation. Hyun Ho Song: Data curation, Formal analysis, Visualization. Jieun Choi: Visualization, Formal analysis, Data curation. Da Woon Jung: Methodology, Investigation, Data curation. Soo Jin Park: Visualization, Formal analysis, Data curation. Ho Jin Park: Visualization, Formal analysis, Data curation. So-Hyeon Park: Formal analysis, Data curation. Da-Eun Kim: Methodology, Validation, Visualization. Gahee Kim: Methodology, Validation, Visualization. Joong-Hyuck Auh: Writing – review & editing, Funding acquisition, Conceptualization. Dong Ha Bhang: Writing – review & editing, Funding acquisition, Conceptualization. Hong Jin Lee: Writing – review &

^b -: no activity observed up to the highest concentration.

editing, Funding acquisition, Conceptualization. **Do Yup Lee:** Writing – review & editing, Writing – original draft, Supervision, Project administration, Funding acquisition, Conceptualization.

Declaration of competing interest

The authors declare that they have no known competing financial interests or personal relationships that could have appeared to influence the work reported in this paper.

Acknowledgments

This research was supported by a grant (20163MFDS120) from Ministry of Food and Drug Safety, by the Bio & Medical Technology Development Program of the National Research Foundation (NRF) funded by the Korean government (MSIT) (No. NRF-2022M3H9A2082952), and by the Basic Science Research Program through the National Research Foundation of Korea funded by the Ministry of Education, Science and Technology (NRF-2021M3A9I4021433).

Appendix A. Supplementary data

Supplementary data to this article can be found online at $\frac{https:}{doi.}$ org/10.1016/j.envint.2024.109184.

Data availability

Data will be made available on request.

References

- Adamski, J., Normand, T., Leenders, F., Monte, D., Begue, A., Stehelin, D., Jungblut, P., De Launoit, Y., 1995. Molecular cloning of a novel widely expressed human 80 kDa 17 β -hydroxysteroid dehydrogenase IV. Biochem. J 311, 437–443.
- Almazroo, O.A., Miah, M.K., Venkataramanan, R., 2017. Drug metabolism in the liver. Clin. Liver Dis. 21, 1–20.
- Bhang, D., Kim, B., Kim, B., Schadler, K., Baek, K., Kim, Y., Hsiao, W., Ding, B., Rafii, S., Weiss, M., 2018. Testicular endothelial cells are a critical population in the germline stem cell niche. Nat. Commun. 9, 4379.
- Blanco, A., Blanco, G., 2017. Medical biochemistry ed eds. Academic Press.
- Broutier, L., Mastrogiovanni, G., Verstegen, M.M., Francies, H.E., Gavarró, L.M.,
 Bradshaw, C.R., Allen, G.E., Arnes-Benito, R., Sidorova, O., Gaspersz, M.P., 2017.
 Human primary liver cancer-derived organoid cultures for disease modeling and drug screening. Nat. Med. 23, 1424–1435.
- Browne, P., Van Der Wal, L., Gourmelon, A., 2020. OECD approaches and considerations for regulatory evaluation of endocrine disruptors. Mol. Cell. Endocrinol. 504, 110675.
- Caipa Garcia, A.L., Arlt, V.M., Phillips, D.H., 2022. Organoids for toxicology and genetic toxicology: applications with drugs and prospects for environmental carcinogenesis. Mutagenesis 37, 143–154.
- Casey, W.; Hattan, D.; Carlson, K.; Jacobs, A.; Bray, J.; Hamm, J.; Ceger, P.; Allen, D.; Stokes, W. ICCVAM Performance Standards for the BG1Luc ER TA Test Method. 2012.
- Chemicals, A.-E. Recombinant Cell Bioassays for Endocrine Disruptors: Development of a Stably Transfected Human Ovarian Cell Line for the Detection of Estrogenic and. In vitro & molecular toxicology 2000;13.
- Christina, Q. OECD/OCDE 455 OECD Guideline for the testing of chemicals performance based test guideline for stably transfected. 2021.
- Clevers, H., 2016. Modeling development and disease with organoids. Cell 165, 1586–1597.
- Denk, H., Abuja, P.M., Zatloukal, K., 2019. Animal models of NAFLD from the pathologist's point of view. Biochimica et Biophysica Acta (BBA)-Mol. Basis Dis. 1865. 929–942.
- Dolegowska, K., Marchelek-Mysliwiec, M., Nowosiad-Magda, M., Slawinski, M., Dolegowska, B., 2019. FGF19 subfamily members: FGF19 and FGF21. J. Physiol. Biochem. 75, 229–240.
- Dutta, D., Heo, I., Clevers, H., 2017. Disease modeling in stem cell-derived 3D organoid systems. Trends Mol. Med. 23, 393–410.
- Elbadawy, M., Yamanaka, M., Goto, Y., Hayashi, K., Tsunedomi, R., Hazama, S., Nagano, H., Yoshida, T., Shibutani, M., Ichikawa, R., 2020. Efficacy of primary liver organoid culture from different stages of non-alcoholic steatohepatitis (NASH) mouse model. Biomaterials 237, 119823.
- Eldridge, C.J.C., Laws, S.C., 2016. The US EPA's Tier 1 Screening Battery for Endocrine Disruptor. Endocrine Toxicology. CRC Press.

- Elsby, R., Maggs, J.L., Ashby, J., Park, B.K., 2001. Comparison of the Modulatory Effects of Human and Rat Liver Microsomal Metabolism on the Estrogenicity of Bisphenol A: Implications for Extrapolation to Humans. J. Pharmacol. Exp. Ther. 297, 103–113.
- Falamarzi, K., Malekpour, M., Tafti, M.F., Azarpira, N., Behboodi, M., Zarei, M., 2022. The role of FGF21 and its analogs on liver associated diseases. Front. Med. 9, 967375.
- Gelbke, H., Kayser, M., Poole, A., 2004. OECD test strategies and methods for endocrine disruptors. Toxicology 205, 17–25.
- Gicquel, T., Pelletier, R., Bourdais, A., Ferron, P.-J., Morel, I., Allard, P.-M., Le Daré, B., 2024. Interest of molecular networking in fundamental, clinical and forensic toxicology: A state-of-the-art review. TrAC Trends Anal. Chem. 117547.
- Grignard, E., Håkansson, H., Munn, S., 2020. Regulatory needs and activities to address the retinoid system in the context of endocrine disruption: the European viewpoint. Reprod. Toxicol. 93, 250–258.
- Hass, U., Ministerråd, N., Råd, N., 2004. OECD Conceptual Framework for Testing and Assessment of Endocrine Disrupters as a basis for regulation of substances with endocrine disrupting properties ed^eds. Nordic Council of Ministers.
- He, Y.-T., Zhu, X.-L., Li, S.-F., Zhang, B.-Q., Li, Y., Wu, Q., Zhang, Y.-L., Zhou, Y.-Y., Li, L., Qi, Y.-N., 2020. Creating rat hepatocyte organoid as an in vitro model for drug testing. World J. Stem Cells 12, 1184.
- Heindel, J.J., Blumberg, B., Cave, M., Machtinger, R., Mantovani, A., Mendez, M.A., Nadal, A., Palanza, P., Panzica, G., Sargis, R., 2017. Metabolism disrupting chemicals and metabolic disorders. Reprod. Toxicol. 68, 3–33.
- Hilborn, E., Stål, O., Jansson, A., 2017. Estrogen and androgen-converting enzymes 17β-hydroxysteroid dehydrogenase and their involvement in cancer: with a special focus on 17β-hydroxysteroid dehydrogenase type 1, 2, and breast cancer. Oncotarget 8, 30552.
- Ho, K.-L., Yuen, K.-K., Yau, M.-S., Murphy, M.B., Wan, Y., Fong, B.M.W., Tam, S., Giesy, J.P., Leung, K.S.Y., Lam, M.H.W., 2017. Glucuronide and Sulfate Conjugates of Bisphenol A: Chemical Synthesis and Correlation Between Their Urinary Levels and Plasma Bisphenol A Content in Voluntary Human Donors. Arch. Environ. Contam. Toxicol. 73, 410–420.
- Huch, M., Dorrell, C., Boj, S.F., Van Es, J.H., Li, V.S., Van De Wetering, M., Sato, T., Hamer, K., Sasaki, N., Finegold, M.J., 2013. In vitro expansion of single Lgr5+ liver stem cells induced by Wnt-driven regeneration. Nature 494, 247–250.
- Inoue, H., Kemanai, S., Sano, C., Kato, S., Yokota, H., Iwano, H., 2016. Bisphenol A glucuronide/sulfate diconjugate in perfused liver of rats. J. Vet. Med. Sci. 78, 733–737.
- Ishigamori, R., Naruse, M., Hirata, A., Maru, Y., Hippo, Y., Imai, T., 2022. The potential of organoids in toxicologic pathology: Histopathological and immunohistochemical evaluation of a mouse normal tissue-derived organoid-based carcinogenesis model. J. Toxicol. Pathol. 35, 211–223.
- Itäaho, K., Mackenzie, P.İ., Ikushiro, S.-I., Miners, J.O., Finel, M., 2008. The configuration of the 17-hydroxy group variably influences the glucuronidation of β-estradiol and epiestradiol by human UDP-glucuronosyltransferases. Drug Metab. Dispos. 36, 2307–2315.
- Jacobs, M., Janssens, W., Bernauer, U., Brandon, E., Coecke, S., Combes, R., Edwards, P., Freidig, A., Freyberger, A., Kolanczyk, R., 2008. The use of metabolising systems for in vitro testing of endocrine disruptors. Curr. Drug Metab. 9, 796–826.
- Jacobs, M.N., Laws, S.C., Willett, K., Schmieder, P., Odum, J., 2013. In vitro metabolism and bioavailability tests for endocrine active substances: what is needed next for regulatory purposes? ALTEX-Alternatives to Animal Experimentation 30, 331–351.
- Jang, Y., Moon, J.H., Jeon, B.K., Park, H.J., Lee, H.J., Lee, D.Y., 2023. Comprehensive Evaluation System for Post-Metabolic Activity of Potential Thyroid-Disrupting Chemicals. J. Microbiol. Biotechnol. 33, 1351.
- Jeon, B.K., Jang, Y., Lee, E.M., Moon, J.H., Lee, H.J., Lee, D.Y., 2021. A systematic approach to metabolic characterization of thyroid-disrupting chemicals and their in vitro biotransformants based on prediction-assisted metabolomic analysis. J. Chromatogr. A 1649, 462222.
- Jia, L., Liu, X., 2007. The conduct of drug metabolism studies considered good practice (II): in vitro experiments. Curr. Drug Metab. 8, 822–829.
- Kahn, L.G., Philippat, C., Nakayama, S.F., Slama, R., Trasande, L., 2020. Endocrinedisrupting chemicals: implications for human health. Lancet Diabetes Endocrinol. 8, 703–718.
- Kim, J., Koo, B.-K., Knoblich, J.A., 2020. Human organoids: model systems for human biology and medicine. Nat. Rev. Mol. Cell Biol. 21, 571–584.
- Kuhl, H., 2005. Pharmacology of estrogens and progestogens: influence of different routes of administration. Climacteric 8, 3–63.
- Labhart, A., 2012. Clinical endocrinology: theory and practice ed^eds. Springer Science & Business Media.
- Lazier, C.B., 1963. The oxidative metabolism of estrogens by mammalian liver. University of British Columbia.
- Li, W.-P., Wang, Y.-F., Gao, J., Yu, M.-L., Tu, Y.-Y., Yao, Y.-Q., 2014. In vitro evidence for endocrine-disrupting chemical (EDC)'s inhibition of drug metabolism. Afr. Health Sci. 14, 185–188.
- Livingstone, C., Borai, A., 2014. Insulin-like growth factor-II: its role in metabolic and endocrine disease. Clin. Endocrinol. 80, 773–781.
- Longcope, C., Gorbach, S., Goldin, B., Woods, M., Dwyer, J., Warram, J., 1985. The metabolism of estradiol; oral compared to intravenous administration. J. Steroid Biochem. 23, 1065–1070.
- Maestri, E., 2021. The 3Rs principle in animal experimentation: A legal review of the state of the art in Europe and the case in Italy. Biotech 10, 9.
- Mandon, M., Huet, S., Dubreil, E., Fessard, V., Le Hégarat, L., 2019. Three-dimensional HepaRG spheroids as a liver model to study human genotoxicity in vitro with the single cell gel electrophoresis assay. Sci. Rep. 9, 10548.

- No, O.T., 2021. 455: performance-based test guideline for stably transfected transactivation in vitro assays to detect estrogen receptor agonists and antagonists. Section, OECD Guidelines for the Testing of Chemicals, p. 4.
- Nokelainen, P., Peltoketo, H., Vihko, R., Vihko, P., 1998. Expression cloning of a novel estrogenic mouse 17β-hydroxysteroid dehydrogenase/17-ketosteroid reductase (m17HSD7), previously described as a prolactin receptor-associated protein (PRAP) in rat. Mol. Endocrinol. 12, 1048–1059.
- Nothias, L.-F., Petras, D., Schmid, R., Dührkop, K., Rainer, J., Sarvepalli, A., Protsyuk, I., Ernst, M., Tsugawa, H., Fleischauer, M., 2020. Feature-based molecular networking in the GNPS analysis environment. Nat. Methods 17, 905–908.
- O'Dell, S.D., Day, I.N., 1998. Molecules in focus Insulin-like growth factor II (IGF-II). Int. J. Biochem. Cell Biol. 30, 767–771.
- OECD. Series on Testing and Assessment: No 150: Guidance document on standardised test guidelines for evaluating chemicals for endocrine disruption. 2012.
- OECD. Revised Guidance Document 150 on Standardised Test Guidelines for Evaluating Chemicals for Endocrine Disruption ed^eds; 2018a.
- OECD. Test No. 319B: Determination of in vitro intrinsic clearance using rainbow trout liver S9 sub-cellular fraction (RT-S9) ed^eds; 2018b.
- Ogoke, O., Maloy, M., Parashurama, N., 2021. The science and engineering of stem cell-derived organoids-examples from hepatic, biliary, and pancreatic tissues. Biol. Rev. 96, 179–204.
- Ooka, M., Lynch, C., Xia, M., 2020. Application of in vitro metabolism activation in high-throughput screening. Int. J. Mol. Sci. 21, 8182.
- Orlowski, M., WILK, S., 1975. Intermediates of the γ-Glutamyl Cycle in Mouse Tissues: Influence of Administration of Amino Acids on Pyrrolidone Carboxylate and γ-Glutamyl Amino Acids. Eur. J. Biochem. 53, 581–590.
- Papalou, O., Kandaraki, E.A., Papadakis, G., Diamanti-Kandarakis, E., 2019. Endocrine disrupting chemicals: an occult mediator of metabolic disease. Front. Endocrinol. 10, 112
- Parada-Bustamante, A.; Valencia, C.; Reuquén, P.; Díaz, P.; Rincion-Rodriguez, R.; A Orihuela, P. Role of 2-methoxyestradiol, an endogenous estrogen metabolite, in health and disease. Mini reviews in medicinal chemistry 2015;15:427-438.
- Park, B., Pirmohamed, M., Tingle, M., Madden, S., Kitteringham, N., 1994. Bioactivation and bioinactivation of drugs and drug metabolites: Relevance to adverse drug reactions. Toxicol. In Vitro 8, 613–621.
- Pearl, P.L., 2013. Monoamine neurotransmitter deficiencies. Handb. Clin. Neurol. 113, 1819–1825.
- Rahimi-Pour, A., Wellman-Bednawska, M., Galteau, M.M., Artur, Y., Siest, G., 1986. Identification of gamma-glutamyltransferase in rat liver plasma membranes after two-dimensional electrophoresis. Electrophoresis 7, 83–88.
- Rahman, M.S., Pang, W.-K., Amjad, S., Ryu, D.-Y., Adegoke, E.O., Park, Y.-J., Pang, M.-G., 2022. Hepatic consequences of a mixture of endocrine-disrupting chemicals in male mice. J. Hazard. Mater. 436, 129236.
- Ramachandran, S.D., Schirmer, K., Münst, B., Heinz, S., Ghafoory, S., Wölfl, S., Simon-Keller, K., Marx, A., Øie, C.I., Ebert, M.P., 2015. In vitro generation of functional liver organoid-like structures using adult human cells. PLoS One 10, e0139345.
- Registre, M., Proudlock, R., 2016. The in vitro chromosome aberration test. Elsevier, Genetic toxicology testing.
- Reichstein, I.S., König, M., Wojtysiak, N., Escher, B.I., Henneberger, L., Behnisch, P., Besselink, H., Thalmann, B., Colas, J., Hörchner, S., 2023. Replacing animal-derived components in in vitro test guidelines OECD 455 and 487. Sci. Total Environ. 868, 161454.
- Reinen, J., Vermeulen, N., 2015. Biotransformation of endocrine disrupting compounds by selected phase I and phase II enzymes–formation of estrogenic and chemically reactive metabolites by cytochromes P450 and sulfotransferases. Curr. Med. Chem. 22, 500–527.
- Rhyu, J., Yu, R., 2021. Newly discovered endocrine functions of the liver. World J. Hepatol. 13, 1611.
- Richardson, J.S., Bai, A., Kulkarni, A.A., Moghaddam, F.M., 2016. Efficiency in drug discovery: liver S9 fraction assay as a screen for metabolic stability. Drug Metab. Lett. 10. 83–90.
- Rinwa, P., Eriksson, M., Cotgreave, I., Bäckberg, M., 2024. 3R-Refinement principles: elevating rodent well-being and research quality. Lab. Anim. Res. 40, 11.

- Roh, H.-S., Kim, D.-E., Kim, G., Kim, J., Fan, D., Kim, H.S., Kim, Y.-H., Lee, J.-H., Kim, B. G., Ryu, M.-O., 2024. Establishment and long-term expansion of adult hepatobiliary organoids co-cultured with liver endothelial cells. Heliyon 10.
- Sakkiah, S., Wang, T., Zou, W., Wang, Y., Pan, B., Tong, W., Hong, H., 2018. Endocrine disrupting chemicals mediated through binding androgen receptor are associated with diabetes mellitus. Int. J. Environ. Res. Public Health 15, 25.
- Schene, I.F., Joore, I.P., Oka, R., Mokry, M., van Vugt, A.H., van Boxtel, R., van der Doef, H.P., van der Laan, L.J., Verstegen, M.M., van Hasselt, P.M., 2020. Prime editing for functional repair in patient-derived disease models. Nat. Commun. 11, 5352.
- Shanle, E.K., Xu, W., 2011. Endocrine disrupting chemicals targeting estrogen receptor signaling: identification and mechanisms of action. Chem. Res. Toxicol. 24, 6–19.
- Skottvoll, F.S., Hansen, F.A., Harrison, S., Boger, I.S., Mrsa, A., Restan, M.S., Stein, M., Lundanes, E., Pedersen-Bjergaard, S., Aizenshtadt, A., 2021. Electromembrane extraction and mass spectrometry for liver organoid drug metabolism studies. Anal. Chem. 93, 3576–3585.
- Stanley, L., 2024. Drug metabolism. Elsevier, Pharmacognosy.
- Tabb, M.M., Blumberg, B., 2006. New modes of action for endocrine-disrupting chemicals. Mol. Endocrinol. 20, 475–482.
- Taxak, N., Bharatam, P.V., 2014. Drug metabolism: A fascinating link between chemistry and biology. Resonance 19, 259–282.
- Uetrecht, J., 2003. Bioactivation. CRC Press, Drug metabolizing enzymes.
- Van den Belt, K., Berckmans, P., Vangenechten, C., Verheyen, R., Witters, H., 2004. Comparative study on the in vitro/in vivo estrogenic potencies of 17β -estradiol, estrone, 17α -ethynylestradiol and nonylphenol. Aquat. Toxicol. 66, 183–195.
- van Vugt-Lussenburg, B.M., van der Lee, R.B., Man, H.-Y., Middelhof, I., Brouwer, A., Besselink, H., van der Burg, B., 2018. Incorporation of metabolic enzymes to improve predictivity of reporter gene assay results for estrogenic and anti-androgenic activity. Reprod. Toxicol. 75, 40–48.
- Vorrink, S. U., Ullah, S., Schmidt, S., Nandania, J., Velagapudi, V., Beck, O., Ingelman-Sundberg, M., Lauschke, V.M., 2017. Endogenous and xenobiotic metabolic stability of primary human hepatocytes in long-term 3D spheroid cultures revealed by a combination of targeted and untargeted metabolomics. FASEB J. 31, 2696.
- Vyas, D., Baptista, P.M., Brovold, M., Moran, E., Gaston, B., Booth, C., Samuel, M., Atala, A., Soker, S., 2018. Self-assembled liver organoids recapitulate hepatobiliary organogenesis in vitro. Hepatology 67, 750–761.
- Wang, B., Tontonoz, P., 2019. Phospholipid remodeling in physiology and disease. Annu. Rev. Physiol. 81, 165–188.
- Wu, F.J., Friend, J.R., Remmel, R.P., Cerra, F.B., Hu, W.-S., 1999. Enhanced cytochrome P450 IA1 activity of self-assembled rat hepatocyte spheroids. Cell Transplant. 8, 233–246
- Yamazaki, H., Shaw, P.M., Guengerich, F.P., Shimada, T., 1998. Roles of cytochromes P450 1A2 and 3A4 in the oxidation of estradiol and estrone in human liver microsomes. Chem. Res. Toxicol. 11, 659–665.
- Yang, S., Hu, H., Kung, H., Zou, R., Dai, Y., Hu, Y., Wang, T., Lv, T., Yu, J., Li, F., 2023. Organoids: The current status and biomedical applications. MedComm 4, e274.
- Yang, P.-W., Jiao, J.-Y., Chen, Z., Zhu, X.-Y., Cheng, C.-S., 2022. Keep a watchful eye on methionine adenosyltransferases, novel therapeutic opportunities for hepatobiliary and pancreatic tumours. Biochimica et Biophysica Acta (BBA)-Reviews on. Cancer 1877, 188793.
- Yilmaz, B., Terekeci, H., Sandal, S., Kelestimur, F., 2020. Endocrine disrupting chemicals: exposure, effects on human health, mechanism of action, models for testing and strategies for prevention. Rev. Endocr. Metab. Disord. 21, 127–147.
- Zercher, M., Coral, J.A., Nabb, D., Powers, G., Jones, A., Johanning, K., 2024.
 A comparison of in vitro metabolic clearance of various regulatory fish species using hepatic S9 fractions. Environ. Toxicol. Chem.
- Zlatnik, M.G., 2016. Endocrine-disrupting chemicals and reproductive health. J. Midwifery Womens Health 61, 442–455.
- Zoeller, R.T., Brown, T.R., Doan, L.L., Gore, A.C., Skakkebaek, N.E., Soto, A.M., Woodruff, T., Vom Saal, F., 2012. Endocrine-disrupting chemicals and public health protection: a statement of principles from The Endocrine Society. Endocrinology 153, 4097–4110.